Volatile distributions in and on the Moon revealed by Cu and Fe isotopes in the 'Rusty Rock' 66095

James M.D. Day, Paolo Sossi, Charles Shearer, Frédéric Moynier

Volatile distributions in and on the Moon revealed by Cu and Fe isotopes in the 'Rusty Rock' 66095

James M.D. Day[1,2*], Paolo A. Sossi[2], Charles K. Shearer[3], Frederic Moynier[2,4]

[1]Scripps Institution of Oceanography, University of California San Diego, La Jolla, CA 92093-0244, USA
[2]Institut de Physique du Globe de Paris, Université Paris Diderot, Sorbonne Paris Cité, 1 rue Jussieu, 75005, Paris, France
[3]Institute of Meteoritics, University of New Mexico, Albuquerque, NM 87131, USA
[4]Institut Universitaire de France, 75005, Paris

*Corresponding author: jmdday@ucsd.edu

Accepted manuscript for *Geochimica et Cosmochimica Acta LAT Special Issue (20 February 2019)*

Abstract Length:	381
Total word count:	6548
Figures:	5
Tables:	2

Keywords: Copper isotopes; iron isotopes; Moon; Rusty Rock; condensates; volatile elements; evaporation

ABSTRACT

The Apollo 16 'Rusty Rock' impact melt breccia 66095 is a volatile-rich sample, with the volatiles inherited through vapor condensation from an internal lunar source formed during thermo-magmatic evolution of the Moon. We report Cu and Fe isotope data for 66095 and find that bulk-rocks, residues and acid leaches span a relatively limited range of compositions (3.0 ±1.3 wt.% FeO [range = 2.0-4.8 wt.%], 5.4 ±3.1 ppm Cu [range = 3-12 ppm], average δ^{56}Fe of 0.15 ± 0.05‰ [weighted mean = 0.16‰] and δ^{65}Cu of 0.72 ± 0.14‰ [weighted mean = 0.78‰]). In contrast to the extreme enrichment of light isotopes of Zn and heavy isotopes of Cl in 66095, δ^{65}Cu and δ^{56}Fe in the sample lie within the previously reported range for lunar mare basalts (0.92 ± 0.16‰ and 0.12 ± 0.02‰, respectively). The lack of extreme isotopic fractionation for Cu and Fe isotopes reflects compositions inherent to 66095, with condensation of a cooling gas from impact-generated fumarolic activity at temperatures too low to lead to the condensation of Cu and Fe, but higher than required to condense Zn. Together with thermodynamic models, these constraints suggest that the gas condensed within 66095 between 700 and 900 °C (assuming a pressure of 10^{-6} and an fO_2 of IW-2). That the Cu and Fe isotopic compositions of sample 66095 are within the range of mare basalts removes the need for an exotic, volatile-enriched source. The enrichment in Tl, Br, Cd, Sn, Zn, Pb, Rb, Cs, Ga, B, Cl, Li relative to Bi, Se, Te, Ge, Cu, Ag, Sb, Mn, P, Cr and Fe in the 'Rusty Rock' is consistent with volcanic outgassing models and indicates that 66095 likely formed distal from the original source of the gas. The volatile-rich character of 66095 is consistent with impact-generated fumarolic activity in the region of the Cayley Plains, demonstrating that volatile-rich rocks can occur on the lunar surface from outgassing of a volatile-poor lunar interior. The 'Rusty Rock' indicates that the lunar interior is significantly depleted in volatile elements and compounds and that volatile-rich lunar surface rocks likely formed through vapor condensation. Remote sensing studies have detected volatiles on the lunar surface, attributing them dominantly to solar wind. Based on the 'Rusty Rock', some of these surface volatiles may also originate from the Moon's interior.

1. Introduction

Knowledge of the origin and distribution of volatile elements in and on the Moon is important for models of Earth-Moon system formation and planetary accretion and differentiation, as well as for understanding volcanism and surface volatile distributions (e.g., Taylor, 2012; Day & Moynier, 2014). Initial work on Apollo samples found that the Moon is depleted with respect to the bulk silicate Earth for elements that are cosmochemically volatile or moderately volatile (e.g., Wolf & Anders, 1980; Jones & Palme, 2000). In this respect, volatile or moderately volatile elements can be defined by the 50% condensation temperatures at gas pressures of $<10^{-4}$ bar of 665 K and 1135 K, respectively (Lodders, 2003). Early measurements of low initial Rb/Sr and high U/Pb ratios for lunar rocks implied an interior devoid of volatile and moderately volatile elements since its inception (Papanastassiou et al., 1970; Tatsumoto & Rosholt, 1970). Stable isotope signatures of Zn (Paniello et al., 2012; Kato et al., 2015), K (Wang & Jacobsen, 2016), Cl (Sharp et al., 2010; Boyce et al. 2016), Cr (Sossi et al. 2018), Ga (Kato & Moynier, 2017) and Rb (Pringle & Moynier, 2017) indicate that evaporation/condensation processes during or following lunar formation control the depletion in these elements. Regardless of when volatile depletion occurred, extreme depletions of volatile elements in lunar rocks, compared with primitive meteorites and Earth, indicate a highly energetic formation process and catastrophic outgassing of the material that formed the Moon (Day & Moynier, 2014; Albarède et al., 2015).

In contrast to evidence for a volatile-depleted Moon, studies of some Apollo lunar crustal rocks have shown modest enrichment in moderately volatile elements (e.g., Krahenbuhl et al., 1973). Lunar pyroclastic glass beads have Pb compositions revealing a source with $^{238}U/^{204}Pb$ (~25) only four times more depleted than Earth's mantle ($^{238}U/^{204}Pb$ = ~6-8; Tatsumoto et al., 1987), while elevated abundances of OH, F, Cl and S in olivine melt inclusions from pyroclastic glass beads and mare basalts indicate that they are volatile-enriched (Hauri et al., 2011; Chen et al., 2014). Water appears to be more depleted in the Moon than in Earth, however. For example, there is no petrographic evidence for water-rich mineral phases such as amphibole in mare basalts, which may relate to their lack of stability (e.g., Sisson & Grove, 1993) due to low contents of

moderately volatile Na and K in mesostasis and bulk lunar igneous rocks. Isotopically light Zn, Cu and Fe compositions also characterize the pyroclastic glasses (Moynier et al., 2006; Herzog et al., 2009; Kato et al., 2015), as well as light Zn in some mare basalts and crustal rocks (Paniello et al. 2012; Kato et al., 2015; Day et al., 2017), indicating volatile-rich vapor condensation. These signatures are inconsistent with complete evaporative loss of volatile elements from the Moon, requiring that some volatile components exist in its interior.

It is now established that volatile deposits occur on the lunar surface. Data from remote sensing missions have identified H-bearing species not only within permanently-shadowed cold traps at polar regions, but also in non-polar regions of the Moon (e.g. Feldman et al., 1998; Pieters et al., 2009; Paige et al., 2010; Colaprete et al., 2010; Li & Milliken, 2017). While much of this volatile-rich material has been attributed to solar wind implantation, some fraction of the volatile inventory may originate from lunar interior sources, even if the interior source was initially volatile-depleted (Day et al., 2017).

To examine the distribution of volatile elements in and on the Moon, we present new Cu and Fe isotope data for the 'rusty rock', 66095. Sample 66095 is notable for several reasons. First, it is a type-example of a volatile-enriched lunar sample, with elevated contents of Bi, Br, Cd, Cl, Ge, I, Pb, Sb, Tl and Zn compared to other lunar samples (Krahenbuhl et al., 1973; Wanke et al., 1981; Jovanovic & Reed, 1981; Ebihara et al., 1992; Day et al., 2017). It is a fine to medium-grained impact melt breccia with elevated highly siderophile element abundances (0.001-0.1 × CI Chondrite; Day et al., 2017) that contains clasts of anorthosite, troctolite and basalt and an incompatible-element rich ['KREEPy'] geochemical signature. Fragments of the impact melt breccia define an ^{87}Rb-^{87}Sr formation age of 4.06 ±0.24 Ga that is identical, within uncertainty, of the ^{207}Pb-^{206}Pb age of 4.01 ±0.06 Ga (Nunes & Tatsumoto, 1973). Initial ^{87}Sr/^{86}Sr for 66095 is 0.69909 ±5, consistent with a source with low long-term time-integrated Rb/Sr (Day et al., 2017), while 85% of Pb in 66095 is unsupported by radioactive decay of U and Th, requiring a high ^{238}U/^{204}Pb (>570) source (Nunes & Tatsumoto, 1973). Second,

the 'rusty' character of 66095 is due to the presence of akaganéite (FeOOH; Taylor et al., 1973) and lawrencite ($FeCl_2$; Shearer et al., 2014). The presence of these minerals has led to the hypothesis that volatile element enrichment occurred in 66095 either through alteration during transit to Earth (Taylor et al., 1973), or through fumarolic activity on the Moon (Krahenbuhl et al., 1973; Nunes & Matsumoto, 1973; Shearer et al., 2014). During fumarolic activity, temperatures and Cl-rich gas compositions inferred for this process are potentially sufficient to mobilize the moderately volatile elements in the vapor phase. Both Fe and Cu tend to form chloro-complexes at low temperatures (<700 °C), whereas the monatomic gas species are stable at magmatic temperatures (Renggli et al. 2017). The stable isotopic fractionation between these different species and the condensed phase can therefore be used to query the nature of vapor deposition observed in 66095. In this study, we examine the isotopic and elemental fractionation of Cu and Fe with respect to other volatile and moderately volatile elements, and the implications for volatiles both in and on the Moon.

2. Sample, leaching/etching and digestion procedures

Three fragments of the 'Rusty Rock', 66095, 421 (163 mg), 66095, 425 (173 mg) and 66095, 430 (201 mg) were used to measure Fe and Cu isotope compositions, with Zn isotope data presented for the samples previously by Day et al. (2017). Samples 66095, 421 and 66095, 430 were dominantly grey crystalline material with no visible clasts, similar to fragments of poikilitic impact melt described previously (Garrison & Taylor, 1980; Hunter & Taylor, 1981). Sample 66095, 425 was composed of pale-colored anorthosite-rich material, with black vitrophyric impact-melt glass. This clast is like the 'cataclastic anorthosite' clasts noted by Garrison & Taylor (1980).

A goal in studying 66095 was to assess isotopic heterogeneity within fragments of the sample, and a procedure of crushing and leaching/etching was designed and performed on samples (Table S1 of Day et al., 2017). These protocols were developed based on previous leaching experiments and observations of volatile element heterogeneity observed in fragments of 66095 (Jovanovic and Reed, 1981). In the first stage, sample 66095, 421 was powdered as a whole-rock sample, with no leaching or

157 modification. Samples 66095, 425 and 66095, 430 were broken into two fragments. One
158 fragment of each of these samples was powdered and digested, with no leaching or
159 modification. These samples make up the 'bulk' measurements given in **Table 1**. The
160 remaining materials, including powder from 66095, 421 and ground fragments from
161 66095, 425 and 66095, 430 were leached and the leachates (labelled as L) and residual
162 fragments (labelled as R) were dried and precisely weighed to calculate concentrations.
163 Drying was performed between each leaching or etching step and was done in a class-10
164 hood at 100˚C. Weighing was done at room temperature (21.5˚C) in Teflon vessels using
165 a Mettler Toledo XPE205 Analytical Balance with repeatability of 0.007 mg.
166
167 Three different leaching/etching experimental processes were used. For aliquots
168 of 66095, 425(B) and 66095, 430 the sample powder was leached for 30 minutes in 18.2
169 MΩ H_2O and the leachate was then separated from the residue (Exp. 1). For aliquots of
170 66095, 421 and 66095, 430, the sample powder was leached for 30 minutes in 1M HCl
171 and the leachate separated from the residue (Exp. 2). Finally, a three-step leaching
172 process was employed on 66095, 421 (Exp. 3). The first step was a 20-minute leach in
173 18.2 MΩ H_2O, with ultra-sonification at 30°C. The H_2O leachate was extracted, and 3M
174 HCl was then added to the residue after dry-down and weighing. This second step was
175 also for 20 minutes, with ultra-sonification at 30°C. When the 3M HCl was extracted
176 from the residue, a strong odor of H_2S was noticeable from all samples. The final etching
177 stage involved addition of 1M HF-HNO_3 after drying of the residue and weighing.
178 Reaction for this final stage took place for 2 hours on a hotplate at 60°C. After extraction
179 of this final leaching stage, samples were dried down, and weighed prior to treatment in
180 an identical fashion for dissolution, as described below. A total of 15 leachates/etchates,
181 residues and whole-rock powders were measured for Fe isotope compositions and
182 abundances, and 10 were analyzed for Cu isotope compositions due to limited available
183 Cu in some of the water leachates.
184
185 After leaching/etching, all samples were dissolved in a 4:1 mixture of ultra-pure
186 HF/HNO_3 in Teflon beakers for 96 hours, dried down and then dissolved and further

dried-down in 6M HCl twice to remove fluorides. Remaining solutions, after Zn column chemistry, were used to obtain Cu and Fe isotopic compositions.

3. Analytical protocols for Cu and Fe isotope analysis

All samples and external standards were purified for Cu isotope analysis using a single column ion chromatographic technique (modified after Maréchal et al., 1999 and used in Sossi et al., 2015). The procedure utilizes Bio-Rad AG1-X8 anion exchange resin, which, at low pH in chloride form, has a high partition coefficient for Cu. Sample aliquots were loaded onto 1 mL of the AG1-X8 (200-400 mesh) resin on 0.4 × 7 cm Teflon columns and matrix elements were eluted in 5 mL of 6 M HCl. The Cu was then eluted in a further 10 ml of 6 M HCl. Iron was then eluted taken in 4 mL of 0.5 M HCl. Samples were evaporated to dryness and the whole procedure was repeated to further purify Cu and Fe. The final purified Cu and Fe fractions were taken up in 0.32 M HNO_3 and made up to 300 ppb and 2 ppm, respectively, and doped with 300 ppb and 5 ppm of Ni, respectively, for analysis.

Copper isotope analysis was performed on a *ThermoScientific* Neptune Plus Multi-Collector Inductively-Coupled-Plasma Mass-Spectrometer (MC-ICP-MS) at the Institut de Physique du Globe, Paris. Samples were introduced into the instrument using an ESI PFA microflow nebuliser (100 µl min^{-1} flow rate) running into a quartz spray chamber following the procedure of Sossi et al. (2015). The instrument was operated at low resolution (m/Δm ~ 450, where Δm is defined at 5 % and 95 % of peak height), with the ^{65}Cu and ^{63}Cu beams collected in the C (central) and L2 Faraday cups respectively. The Ni masses (^{60}Ni, ^{61}Ni, ^{62}Ni) were collected in cups L3, L2 and L1, respectively. Under typical running conditions, a 300 ppb Cu solution generated a 0.06-0.08 nA ion beam (6-8 V total signal using 10^{11} Ω resistors). To ensure sufficient counting statistics on the $^{62}Ni/^{60}Ni$ ratio, the ^{62}Ni signal was kept above 0.5 V. Instrument background signal (typically <10 mV ^{63}Cu) was measured at the beginning of each analytical session. The total procedural blank contained ~1 ng Cu, which equates to <1 % of the Cu sample analyte. Isotope ratios were measured in static mode, with each measurement consisting of 30 cycles of 4.194 second integrations, with a 1 second idle time. Ratios were

calculated in the Thermo Neptune Data Evaluation software, which discarded any outliers at the 2-sigma confidence level. To correct for instrumental mass bias, isotope measurements were calculated using the standard sample bracketing protocol relative to the NIST SRM976 standard and corrected for by using the $^{62}Ni/^{60}Ni$ ratio using the exponential law. Variations in Cu ratios are defined using the delta notation $\delta^{65}Cu$ as follows: $\delta^{65}Cu = [(^{65}Cu/^{63}Cu_{sample}/^{65}Cu/^{63}Cu_{SRM976}) - 1] \times 1000$. Analysis of two separate digestions of USGS standard reference material BHVO-2 gave $\delta^{65}Cu$ of 0.07 ± 0.06‰ (2SE), in good agreement with literature data (Savage et al., 2015; Moynier et al. 2017).

Iron isotope measurements follow the protocol of Sossi et al. (2015). Solutions were diluted to 2 ppm, doped with 5 ppm of Ni, and aspirated through a 100µL/min glass nebulizer into a Scott Double Pass-Cyclonic spray chamber coupled to the *ThermoScientific* Neptune Plus MC-ICP-MS. Forty integrations of 4.194 s were performed on the iron shoulder of the peak with medium resolution slits, affording a resolving power, m/Δm, of 8000; a necessity given the polyatomic ArN, ArO and ArOH interferences that otherwise over-lap with ^{54}Fe, ^{56}Fe and ^{57}Fe respectively. This set-up gave signal intensities of 0.8V for ^{57}Fe and 1V for ^{61}Ni, where Ni corrects for mass bias using the exponential law. The procedural blank for Fe was ≈10 ng and resulted in negligible blanks for most of the samples analyzed. Samples were bracketed against the IRMM-014 standard, yielding the delta value: $\delta^{x}Fe$ (‰) = $([^{x}Fe/^{54}Fe]_{sample}/[^{x}Fe/^{54}Fe]_{IRMM-014} - 1) \times 1000$, where x is equal to ^{56}Fe or ^{57}Fe. All uncertainties reported on the isotope analyses are the standard deviation of replicates. The total procedural external uncertainty is ±0.02 (SE) $\delta^{56}Fe$ based on processing and analysis of standard rock powders. Data for standard ETH Hematite, $\delta^{56}Fe$ = +0.51 ± 0.02‰, $\delta^{57}Fe$ = +0.75 ±0.02‰, agrees with compiled values (Poitrasson et al. 2013).

4. Results

Copper and Fe isotope and abundance results are presented in **Tables 1** and **2** and Cu data is shown in **Figure 1**. Bulk samples of 66095 have concentrations of Cu of 4.7 and 6.3 µg g^{-1}, in good agreement with ICP-MS data (3.6-5.4 µg g^{-1}), with $\delta^{65}Cu$ of 0.70 and 0.79‰. Residue samples generally have a lower range of Cu abundances (2-4.3 µg g^{-}

249 ^{1}; except residue J14 at 18.5 μg g^{-1}) and δ^{65}Cu of between 0.59 and 0.77‰. Leaches and
250 etches of HCl and HF-HNO_3 have a range in Cu abundances (2.5-11.6 μg g^{-1}) and a wide
251 range in δ^{65}Cu of between 0.63 and 1.38‰. None of the water leaches analyzed for Fe
252 and Zn were analyzed for Cu isotopes due to low total Cu contents.
253
254 Iron isotope and abundance results are presented in **Figures 2** and **3**. All data are
255 mass-dependent in δ^{56}Fe-δ^{57}Fe space conforming to δ^{57}Fe (and its uncertainty) ≈1.5 ×
256 δ^{56}Fe. Iron abundance results obtained on purified Fe fractions for MC-ICP-MS agree
257 well with ICP-MS solution data (**Table 1**), except for a single 1M HCl leach for 66095,
258 430. Bulk samples of 66095 have between 2.2 and 4.8 wt.% FeO and a range of δ^{56}Fe
259 between 0.14 to 0.26‰. Residue samples have lower FeO contents (1.6-2.6 wt.%) and a
260 more restricted range of δ^{56}Fe (0.10 to 0.15‰). Leaches and etches of HCl and HF/HNO_3
261 give the widest range of FeO contents (2.3-24.6 wt.%) and heavier δ^{56}Fe (0.15 to 0.19‰)
262 than associated residues. Water leaches have a range in FeO contents (4.0-8.6 wt.%) and
263 the lightest δ^{56}Fe for the dataset (-0.05 to 0.04‰).
264
265 Copper and iron isotopes in 66095 show a much larger relative range in isotopic
266 compositions than for Zn in the same samples. Zinc abundances vary dramatically in
267 whole-rocks, leaches/etches and residues (14.8 to >10,000 μg g^{-1}), but Zn isotopic
268 compositions are generally consistent (-13.5 ±0.3‰, 1SD, n = 12), except for in the water
269 leaches (-13.3 to -8.1‰). None of the measured isotope systems (Fe, Cu, Zn) are
270 correlated with each other for the data set as a whole, or for the bulk, residue or leachate
271 fractionations. Mass balance reconstruction of leachate/etchate and residue experiments
272 versus bulk rock samples of 66095 generally agree well (**Table 2**), with any disagreement
273 likely relating from modal effects between samples, where sample sizes were non-
274 representative of the bulk composition of 66095.
275
276 **4. Discussion**
277 ***4.1 Copper and iron isotope composition of 66095 and the Moon***
278 Prior to discussing the distribution of moderately volatile elements in the Rusty
279 Rock, 66095, it is useful to place the Cu and Fe isotope compositions in context with

lunar compositions. In the first instance, while there is a meteoritic component in the Rusty Rock, the amount of impact contamination is not enough to explain either the Cu or Fe contents of 66095 (Day et al., 2017). Instead, the Moon provides a key comparison with the composition of the Earth, with prior work indicating strong geochemical similarities between the two bodies (Ringwood & Kesson, 1977; O'Neill, 1991). For example, Li, O, Si, Mg, Ca, Ti, Fe, and Sr stable isotopic compositions for the Earth and Moon are all identical within analytical uncertainties (e.g., Spicuzza et al., 2007; Liu et al., 2010; Moynier et al. 2010; Sedaghatpour et al., 2013; Valdes et al., 2014; Day et al., 2016; Millet et al., 2016; Young et al., 2016; Sossi & Moynier, 2017). For moderately volatile elements such as S, Cl, K and Zn, however, the Moon is highly distinctive compared with Earth (e.g., Day & Moynier, 2014, Wang and Jacobsen 2016). To date, there are limited Cu isotopic data available for lunar rocks and therefore the composition of the bulk silicate Moon (BSM) is not well-constrained, while the BSM δ^{56}Fe composition has been estimated from lunar Mg-suite rocks at +0.05 ± 0.02‰ (Sossi & Moynier, 2017); indistinguishable to slightly heavier than bulk silicate Earth (BSE) values of +0.03 ±0.03‰ (Craddock et al., 2013) and +0.05 ± 0.01‰ (Sossi et al., 2016). The estimated BSM δ^{56}Fe value from the Mg-suite samples is ~0.07‰ lighter than the low-Ti mare basalt average of +0.12 ± 0.02‰ (Liu et al. 2010; **Figure 3**), reflecting iron isotopic fractionation of melts from the lunar interior during magmatic differentiation processes (see discussion in Sossi and Moynier, 2017).

As a comparison for the Cu isotopic composition, we compiled data from the literature for a range of lunar rock types, including regolith or soil samples, mare basalts and pyroclastic glass beads that collectively span a wide-range of δ^{65}Cu values (-1 to +4.5‰) and Cu concentrations (2.7 to 84 μg g^{-1}; **Figure 1**). Lunar soil samples are consistently isotopically heavy for both δ^{65}Cu (+0.3 to +4.5‰) and δ^{66}Zn (+2.2 to +6.4‰), with generally low Cu abundances (3 to 84 μg g^{-1}); these characteristics of lunar soils have previously been attributed to impact gardening and sputtering effects (Herzog et al., 2009). The pyroclastic glass beads (74001, 74220) have typically higher Cu abundances (average = ~20 μg g^{-1}) and isotopically lighter δ^{65}Cu (0.15 to –1‰) and δ^{66}Zn compositions than most basalts, which reflect addition of isotopically light Cu- and

311 Zn-rich condensate material to these deposits (Moynier et al., 2006; Herzog et al., 2009;
312 Kato et al., 2015; Day et al., 2017). Mare basalts span a range of Cu abundances (~2.7 to
313 26 μg g^{-1}) exceeding abundances for the most primitive mare basalts (Day, 2018), and
314 have δ^{65}Cu values between -0.1 and 2.0‰.
315
316 It has previously been assumed that mare basalts are proxies for lunar mantle Zn
317 isotope compositions (e.g., Paniello et al., 2012). Making a similar assumption for Cu,
318 pristine mare basalts should have low Cu. This is because Cu content is predicted to be
319 low in the lunar mantle, and hosted within sulfide phases (O'Neill, 1991). Sulfide
320 exhaustion in the lunar mantle occurs after around 8% partial melting due to low S
321 contents, leading to the prediction that low Cu contents occur in primary lunar mantle
322 melts (<10 μg g^{-1}; Day, 2018). Mare basalts with low Cu contents have δ^{65}Cu = +0.92
323 ±0.16‰. This composition is significantly isotopically heavier than typical terrestrial
324 igneous rock compositions (–0.07 to +0.16‰), or the BSE estimate (+0.07 ±0.10‰; 2
325 S.D.; Savage et al., 2015). The heavier estimated δ^{65}Cu of lunar mare basalt sources
326 relative to the BSE is similar to the differences observed for Rb, Cl, K, Zn and S isotopes
327 in the Moon, and consistent with high-temperature processing implied by the depletion in
328 moderately volatile elements in the lunar interior compared with the terrestrial mantle
329 (Day & Moynier, 2014; Wang & Jacobsen, 2016; Pringle & Moynier, 2017).
330
331 It has previously been shown that 66095 is depleted in the heavier isotopes of Zn,
332 distinguishing it from mare basalt compositions (Day et al., 2017). It is therefore
333 remarkable that bulk sample, residue and acid reagent treatments (HCl, HF-HNO_3) of
334 66095 are broadly within the range of lunar mare basalt values for δ^{65}Cu and δ^{56}Fe (or
335 δ^{57}Fe) and Cu concentrations. The only materials from 66095 that show values
336 significantly outside of these ranges are the isotopically heavy bulk breccia sample
337 (66095, 430), and the isotopically light water leach treatments for iron isotopes. For the
338 water leaches, it is likely that they accessed soluble and isotopically light FeCl salts, or
339 akaganéite.
340

The heavy Fe isotopic value in 66095, 430 relates to the highest Fe content of the dataset and is consistent with sampling of impact-generated Fe-metal grains formed by partial impact-vaporization and preferential loss of light Fe isotopes, as proposed previously by Wang et al. (2012). Prior work on terrestrial analog systems have demonstrated that large (2-3‰) Fe isotope fractionations occur due to redox reactions between ferrous and ferric species (e.g., Hill & Schauble, 2008; Polyakov & Soultanov, 2011; Syverson et al., 2017). However, in the case of the Moon, where the majority of Fe speciation is considered to be ferrous (Fe^{2+}) or native (Fe^{0}), such fractionations are likely to be of lower relevance. Theoretical studies indicate that changes in bond partners (i.e., different ligands or coordination numbers) should result in significant isotopic fractionation, but conditions similar to those attained on airless bodies have not been well-constrained. Empirical stidy of nanophase iron ($_{np}Fe^{0}$) show large enrichments in the heaviest Fe isotopes (δ^{56}Fe up to 0.71%) compared with lunar mare basalts (Wang et al., 2012). These results indicate that impact vaporization processes can lead to enrichment of heavy Fe isotopes in the residues and light Fe isotopes in the vapor, consistent with the Fe isotopic variations in components of 66095 and its origin as an impact melt breccia. Further experiments would be valuable to elucidate this effect.

Mass-balance calculations for leaching and residue experiments yield similar values to bulk samples of 66095 (**Table 2**), with 3.0 ±1.3 wt.% FeO (range = 2.0-4.8 wt.%), 5.4 ±3.1 ppm Cu (range = 3-12 ppm), with average δ^{56}Fe of 0.15 ± 0.05‰ (weighted mean = 0.16‰) and δ^{65}Cu of 0.72 ±0.14‰ (weighted mean = 0.78‰). The new results for Cu and Fe isotope compositions of 66095 show that they are not particularly anomalous relative to baseline lunar compositions defined by mare basalts (δ^{65}Cu = +0.92 ± 0.16‰; δ^{56}Fe = +0.12 ± 0.02‰). In the following sections, we outline the importance of these observations for volatile element behavior in and on the Moon.

4.2 Origin of volatile element enrichments in the Rusty Rock, 66095

The fine-grained subophitic to ophitic polymict breccia 66095, is the archetypal lunar ‘Rusty Rock’, recognized as an important sample during initial characterization with the discovery of rust coloured stains on its surface and interior (Bass, 1972; Taylor

et al., 1973; El Goresy et al., 1973). The 'rusty' character of 66095 is due to the presence of akaganéite (FeOOH; Taylor et al., 1973) and lawrencite ($FeCl_2$; Shearer et al., 2014). Subsequently, greater than twenty-five Apollo 16 samples have been identified as having rusty rims of iron hydroxide phases around FeNi metal, as FeO(OH) polymorphs (akaganéite, βFeO[OH,Cl]) (Colson, 1992; Jean et al., 2016). These samples come from nearly all sampled stations of the Apollo 16 mission to the Cayley Plains and include rake samples in soils (68501, 68441), regolith breccias (60016, 61135, 65095, 66035, 66036), polymict or dark matrix breccias (60255, 66055, 69935), impact melt rocks and breccias (60625, 63585, 64455, 64567, 66095), and anorthosite and anorthositic breccias (65326, 67016, 67455). The presence of rusty alteration both within different rock types from the Apollo 16 site, and from different locations across the site suggests a common process responsible for the alteration.

In addition to the pervasive low temperature, volatile-rich oxyhydrated mineral assemblages, 66095 is also enriched in a volatile component, including elevated abundances of Bi, Br, Cd, Cl, Ge, I, ^{204}Pb, Sb, Tl and Zn compared with other lunar samples (Krahenbuhl et al., 1973; Wanke et al., 1981; Jovanovic & Reed, 1981; Ebihara et al., 1992; Day et al., 2017). Amongst these elements, the chlorine composition of 66095 is isotopically heavier ($\delta^{37}Cl$ = +14.0 to +15.6‰) than any known terrestrial rock samples (typically -3 to +3‰), and consistent with $\delta^{37}Cl$ values (+5.6 to +15.7‰) for lunar rocks and soils around the Apollo 16 site (Shearer et al., 2014). The Rusty Rock also has one of the most extreme, isotopically light Zn compositions measured for any Solar System material ($\delta^{66}Zn$ = -13.5‰; Day et al., 2017), again inconsistent with a terrestrial origin, where $\delta^{66}Zn$ is typically between 0.1 and 0.4‰ in terrestrial rocks (Paniello et al., 2012; Moynier et al., 2017).

Amongst the volatile elements, the U-Pb and Rb-Sr isotope systems are tracers *par excellence* of volatile enrichment and depletion since they can both potentially provide chronological information, and, in the case of the U-Pb isotope system, the parent (U) is refractory, and the daughter (Pb) is volatile, whereas the opposite is true for the Rb-Sr isotope system. The lead isotopic composition of 66095 shows that greater than

85% of Pb is unsupported in the rock, identifying a source with high-μ ($^{238}U/^{204}Pb \geq 570$; Nunes & Tatsumoto, 1973). The age defined from ^{207}Pb-^{206}Pb chronology (4.01 ±0.06 Ga) is identical within uncertainty of the ^{87}Rb-^{87}Sr age (4.06 ±0.24 Ga), with the defined $^{87}Sr/^{86}Sr$ initial of 0.69909 ±5, consistent with lunar origins for both isotope systems (Day et al., 2017).

Strontium and Pb isotope compositions suggest a long-term volatile-depleted source for 66095, in apparent contradiction to the enrichment in volatile components in the sample (e.g., Bi, Br, Cd, Cl, Ge, I, ^{204}Pb, Sb, Tl, Zn). These geochemical characteristics can be reconciled by outgassing of an already volatile-depleted source within the Moon to generate the volatile enriched character of 66095 (Day et al., 2017). Such a model is consistent with fumarolic activity (e.g., Krahenbuhl et al., 1973; Nunes & Tatsumoto, 1973), where lawrencite was deposited at between 650˚C to 570˚C (Shearer et al., 2014) and sphalerite was deposited at between 200˚C and 600˚C (Day et al., 2017) from an H-poor gas phase. Shearer et al. (2014) further proposed that the low H gas phase was metal chloride bearing, depositing Zn, Cu, Pb and Fe. In detail, however, the cause of Zn and Pb volatile enrichment must be distinct from Cu and Fe in 66095, based on stable isotope composition. The 'rusty' character and volatile element enrichment of 66095 is therefore consistent with volatile enrichment through fumarolic activity – likely during impact processes - from a volatile-poor source in the Moon, as opposed to partly to fully representing terrestrial alteration products, as had been suggested previously (Epstein & Taylor, 1974; Taylor et al., 1974).

4.3 Causes of Fe, Cu, Pb and Zn isotopic and abundance variability in 66095

A notable feature of the new Cu and Fe isotope data for 66095 is that the values for bulk samples, residues after leaching and HF/HNO_3 treatment samples generally all lie within or close to the range of mare basalts (**Figures 1** and **3**).

To compare the relative enrichments of elements in 66095, data for Cl from Shearer et al. (2014), Sb, Se, Te, Ag, Br, Bi, Cd and Tl from Krahenbuhl et al. (1973) and data for all other elements from Day et al. (2017), are compared with the average lunar

volatile depletion trend (**Figure 4**). A notable aspect of this plot is that two distinct groups of moderately volatile elements (here defined as elements with $T_c50\%$ < Fe) can be distinguished; those that are equally or more depleted than the average lunar volatile depletion trend (Bi, Se, Te, Ge, Cu, Ag, Sb, Mn, P, Cr) and those that are significantly more enriched compared to this trend (Tl, Br, Cd, Sn, Zn, Pb, Rb, Cs, Ga, B, Cl, Li). Concentrations of moderately volatile elements (e.g., Cr, Mn, Cu, Rb, Cs, Zn) measured on different aliquots of 66095 can vary significantly (e.g., Krahenbuhl et al., 1973; Wanke et al., 1981; Ebihara et al., 1992, and see Table S2 of Day et al., 2017), but the same general trends are observed no matter which data are used, suggesting that the observation of two groups of depleted and enriched moderately volatile elements (MVE) is robust.

Instead of the original description of 66095 being enriched in Bi, Br, Cd, Cl, Ge, I, ^{204}Pb, Sb, Tl, Zn, we redefine the moderately volatile enrichment as occurring for Tl, Br, Cd, Sn, Zn, Pb, Rb, Cs, Ga, B, Cl, Li (enriched MVE) and that Bi, Se, Te, Ge, Cu, Ag, Sb, Mn, P and Cr are all relatively depleted (depleted MVE), compared with the average lunar depletion trend. There are two likely reasons for the differences in the relative enrichment of depletion of these MVE with 66095. First, some of the depleted MVE group are inherent to the sample, being dominantly located within minerals and phases associated with the breccia and clasts making up 66095, rather than as condensates. This can be demonstrated for Fe, where the dominant Fe-rich phase in the Rusty Rock are olivine (~10 modal %; Fo_{77}), pyroxene (~30 modal %; $Wo_7En_{72}Fs_{20}$ to $Wo_{17}En_{65}Fs_{18}$), and FeNi metal (~1.2 modal %; Lunar Compendium). Components that make up 66095 are generally low in FeO (1.4-9.6 wt.%; Wanke et al., 1981; this study) and the mass balance for Fe can therefore be fully accounted for by these phases. Metal phases are the dominant source of Cu, where Cu solubility in sphalerite is low (Scott, 1983), and FeNi metal in some Apollo 16 impact melt rocks have up to 0.5 wt.% Cu (McIntosh et al., 2018). Even assuming the average Cu content of FeNi metal grains in impact melt rocks of ~0.1 wt.% Cu, 1.2 modal% FeNi metal in 66095 would give ~12 ppm Cu in bulk samples of 66095, which is well within the range of Cu contents measured for the 'Rusty Rock' (**Table 1**).

The second reason for different distributions of moderately volatile elements in 66095 is due to the role of condensate and vapor deposition, where the enriched MVE group are presumed to have been primarily enriched by such a process. As noted previously, sphalerite and lawrencite were deposited between 200 and 650°C, which would be consistent, for example, with deposition of discrete grains of (Zn,Fe)S or PbS (?) and (Fe,Ni)Cl_2. While some elements appear to be dominantly controlled by primary phases, leaching and etching experiments have the potential to reveal possible condensate or vapour additions, one example being the water leaches measured for Fe isotope compositions (**Table 1**). These water leaches are all isotopically light with respect to Fe (δ^{56}Fe = 0.04 to -0.05‰) and have low total abundances of Fe (0.7 to 20 µg g^{-1}). The low δ^{56}Fe do not reflect analytical blanks, which represent less than 1.4% of the total measured Fe in the samples. The water leach iron isotope compositions are also mass-dependent. Although an extremely minor component of 66095, there appears to be isotopically light Fe within or on 66095, and this may originate from FeCl salts, either directly, or from the breakdown of lawrencite in H_2O, where water leaches have high concentrations of both Fe and Ni (c.f., Table S2 of Day et al., 2017). Examples of location of elements within 66095 and how they were inherited in the sample are given in **Figure 5**, where primary grains of FeNi metal – hosts to both Fe and Cu - are distinct from the secondary sphalerite and veins and infilled fractures of Cl-rich materials.

The composition of moderately volatile elements in the 'Rusty Rock' would imply that it formed at lower temperatures away from a fumarolic vent, consistent with lawrencite and sphalerite thermometry (Shearer et al., 2014; Day et al., 2017). The distribution of moderately volatile trace elements in the 'Rusty Rock', 66095, appear to follow the expected trend of element deposition from a lunar volcanic gas. Renggli et al. (2017) calculated the speciation of Ni, Fe, Cu, Ga, Zn and Pb for a lunar volcanic gas composition at 2 log units below the Iron-Wüstite buffer over a range of temperatures (500 to 1500°C and pressures (10^{-6} to 1 bar). For a lunar composition gas, the major volatiles were likely to be CO, H_2, H_2S, COS and S_2. These authors concluded that deposition with decreasing temperature and increasing pressure occurs in the order: Ni ≈

Fe > Cu > Ga > Zn > Pb. In general, at 10^{-6} bar, these metals exist as monatomic gases at higher temperatures, whereas the gaseous chloride species of Cu and Fe become predominant below 800 °C. As such, native metals tend to precipitate close to the volcanic or fumarolic vent at higher temperatures, with sulfide or chloride species distributed further away. The composition of moderately volatile elements in the 'Rusty Rock' would imply that it formed at lower temperatures away from a fumarolic vent, consistent with the lawrencite and sphalerite thermometry (**Figure 4**). Iron is present as chlorides and oxy-hydroxides that are only stable at low temperatures (<700 °C), implying the persistence of iron in the vapour below 1200-1300 °C as modelled by Renggli et al. (2017). The fact that the Cu and Fe isotope composition of the Rusty Rock is within the range of mare basalts leaves two options. First, that Cu and Fe were not transported in the gas and are instead dominated by inherent mineralogical components, and second that the Cu and Fe budget of the rock condensed entirely and was thus associated with negligible isotope fractionation with respect to its source.

The first option is consistent with the observation that Cu and Fe are not enriched with respect to mare basalts (**Figure 4**). However, that Fe-rich and isotopically light deposits occur on the surface from water leaches attests to some transport of Fe (and the more volatile Cu) in the vapor phase. As discussed above, the quantity that these surface deposits comprise of the total Cu and Fe budget of the rock is minor, and the leachates are not significantly fractionated relative to the bulk rock dissolution. This implies that, although Cu and Fe were transported in the vapor, they were not sufficiently enriched to modify the composition of the bulk rock. Moreover, that the leachates have compositions overlapping with mare basalts argues that the budget of Cu and Fe in the vapor suggests that they condensed fully from the vapor phase such that their isotopic composition should reflect that of their sources (option 2). Therefore, the lunar source from which the vapour was derived was similar in nature to that of mare basalts. Therefore, a distinct, isotopically-fractionated, volatile-enriched reservoir in the lunar mantle in unlikely.

The isotopically 'normal' nature of Cu and Fe in sample 66095 is seemingly at-odds with the strongly fractionated Zn isotope composition (-13.6±0.3 ‰) in the same

sample. A possible explanation for the distinct behavior of Zn relates to its volatility; Zn (and Pb) is calculated to precipitate from a gas of lunar composition at lower temperatures than are Cu and Fe (Renggli et al. 2017). Therefore, the strongly negative δ^{66}Zn implies condensation of the gas at temperatures at which Zn is only partially condensed, resulting in isotopically light condensates. This temperature must have been sufficiently low to have permitted complete condensation of Cu and Fe and to have stabilized Fe-chlorides. Together, these constraints imply precipitation of the gas phase below 900 °C but above 700 °C (at total pressures of 10^{-6} bar and IW-2). That Cu and Fe elements are not enriched in the sample supports lower abundance in the gas phase relative to the source rock. By contrast, that Zn (and Pb) are enriched points to their higher relative abundance in the gas phase compared to the sample, even if Zn has only undergone partial condensation. This scenario would predict strong mass-dependent isotopic fractionation in elements more volatile than Zn, such as Pb, and others that are enriched in sample 66095 (Tl, Cd; **Figure 4**). Gallium isotopes may be particularly exacting because Ga is predicted to condense at temperatures between those of Cu and Zn.

4.4 Implications for volatile reservoirs at the surface and in the lunar interior

The Rusty Rock, 66095, is one of the most volatile-rich rocks recovered from the Moon, having experienced modification by fumarolic activity resulting in the enrichment in some volatile and moderately volatile elements (Krahenbuhl et al., 1973; Nunes & Tatsumoto, 1973). The source of these volatiles, however, is quite volatile-poor, being particularly evident from combined Zn, Cl, Pb and ^{87}Sr/^{86}Sr isotope data indicating addition of condensate material with isotopically heavy Cl, isotopically light Zn, low long-term Rb/Sr and unsupported Pb (Day et al., 2017). The high Zn content and extremely isotopically light δ^{66}Zn are particularly notable features of 66095, making the sample distinct from all other lunar rocks. Here we have shown that for Fe and Cu isotopes, 66095 is not particularly anomalous compared with mare basalts, with these isotope systems being controlled by Fe and Cu within FeNi metal and/or silicate phases within the sample, rather than from phases introduced by fumarolic activity (e.g., sphalerite, Cl in veins). These observations have two important implications, the first

relating to volatile-rich pyroclastic glass beads, and the second to the distribution of volatile elements on the lunar surface.

The pyroclastic glass beads (15426, 74220) are volatile-rich samples from the Moon that were formed by fire fountaining and have high Cu (7 to 32 ppm) and Zn (50 to 230 ppm) concentrations and isotopically light Cu (δ^{65}Cu = +0.1 to -1‰) and Zn (δ^{66}Zn = −1‰ to −4‰) that correlate with bead size (Herzog et al., 2009; Kato et al., 2015). The Zn and Cu isotope compositions in these samples reflect condensates on the surfaces of the beads, as there are no phases dominantly controlling Cu or Zn in the samples, and with direct observation of Zn-bearing minerals on the outsides of the beads (Ma & Liu, 2019). The volcanic glasses have been shown to have significant enrichments in volatile elements that are surface correlated (Krahenbuhl, 1980), with lower estimated μ (^{238}U/^{204}Pb = 19 to 55) than mare basalts (300 to 600; Tatsumoto et al., 1987), and high δ^{37}Cl in leachates from 74220 (+8.6 to +9.6‰; Sharp et al., 2010). The volcanic glasses also have chondritic relative abundances of the HSE on their outer edges (Walker et al., 2004), with absolute abundances of these elements that are greater than in mare basalts (Day et al., 2007; Day & Walker, 2015). Collectively, these lines of evidence suggest that the volcanic glass beads have lunar condensate, as well as impactor materials, on their surfaces, both for Zn, as well as for Cu. The information on volatile contents in the Rusty Rock 66095 indicates that such material was likely added during fire fountaining, or after the formation of the glass bead deposits. The new results for Cu in 66095 would therefore suggest that the lunar pyroclastic glass beads are anomalously enriched in a condensate volatile component from a dominantly 'dry' lunar interior.

A volatile-rich lunar surface has been inferred from remote sensing mission data, including Clementine, Lunar Prospector, Lunar Reconnaissance Orbiter (LRO), the Moon Mineralogy Mapper (M^3) on Chandrayaan-1, and the Lunar Crater Observation and Sensing Satellite (LCROSS). Data from these missions have been used to identify H-bearing species not only within permanently-shadowed cold traps at polar regions, but also in non-polar regions of the Moon (e.g. Feldman et al., 1998; Pieters et al., 2009; Paige et al., 2010; Colaprete et al., 2010; Li & Milliken, 2017). Most of this volatile

component has been attributed to solar wind implantation during agglutinate formation (Li & Milliken, 2017). The 'Rusty Rock' 66095 offers the possibility that a significant fraction of volatiles trapped within some lunar regolith may originate from interior sources and is isotopically strongly fractionated due to the volatile depleted nature of the lunar interior. The fumarolic activity required to form the volatile enriched 'Rusty Rocks' at the Cayley Plains may not be a localized feature, or a temporally limited event, with recent disturbance structures attributed to outgassing occurring at Ina Crater (e.g. Schultz et al., 2006). Testing what fraction of lunar volatile deposits originate from the interior of the Moon should be possible using isotopic fingerprinting of solar wind implantation versus kinetic isotopic fractionation during vapour-phase and condensate reactions.

5. Conclusions

Copper and iron isotope and abundance compositions measured in bulk-rocks, residues and acid leaches span a relatively limited range of compositions (3.0 ±1.3 wt.% FeO [range = 2.0-4.8 wt.%], 5.4 ±3.1 ppm Cu [range = 3-12 ppm], average δ^{56}Fe of 0.15 ± 0.05‰ (weighted mean = 0.156‰) and δ^{65}Cu of 0.72 ±0.14‰ (weighted mean = 0.78‰). The stable isotope compositions of Cu and Fe are similar to averages of mare basalts (δ^{65}Cu = +0.92 ±0.16‰; δ^{56}Fe = +0.12 ± 0.02‰) and are therefore less extreme compositional variations than previously measured for δ^{66}Zn (-13.5 ±0.3‰), δ^{37}Cl (+14 to +15.6‰). Combined with the high ^{206}Pb/^{204}Pb and low ^{87}Sr/^{86}Sr measured in 66095, these results are consistent with the enrichment in volatile elements in the 'Rusty Rock' by fumarolic activity and preferential enrichment of volatiles elements from a cooling gas originating from a volatile-poor lunar interior. We find that the enrichment in Tl, Br, Cd, Sn, Zn, Pb, Rb, Cs, Ga, B, Cl, Li relative to Bi, Se, Te, Ge, Cu, Ag, Sb, Mn, P, Cr and Fe is consistent with volcanic outgassing models, and indicates that 66095 may have formed distal from the original source of the gas. The evidence for impact brecciation and the moderately elevated HSE contents of 66095 are consistent with fumarolic activity in the vicinity of the Apollo 16 site at the Cayley Plains, induced by impact heating. The elucidation of the volatile-rich character of 66095 explains the 'rusting' and alteration on the sample, through fumarolic activity, alteration and deposition of volatile and moderately volatile elements, as well as demonstrating that volatile-rich rocks can occur

620 on the lunar surface from outgassing of the volatile-poor lunar interior. Our results for Cu
621 and Zn isotopes demonstrate that the phases hosting these elements can play an important
622 role in dictating isotopic composition, leading to apparently 'mixed messages' regarding
623 the source of volatiles in lunar samples.
624
625 **Acknowledgements**
626 We dedicate this manuscript to the memory of Lawrence A. Taylor who held a
627 fascination with the Rusty Rock, 66095, throughout his career studying the Moon. We
628 thank the NASA curation staff and CAPTEM for samples. Comments by C. Renglli, A.
629 Ruzicka and two anonymous reviewers are gratefully acknowledged. This work was
630 supported by the NASA Emerging Worlds program (NNX15AL74G) and an IPGP
631 Visiting Professor position to JD. FM acknowledges funding from the European Research
632 Council under the H2020 framework program/ERC grant agreement #637503 (Pristine),
633 as well as financial support of the UnivEarthS Labex program at Sorbonne Paris Cité
634 (ANR-10-LABX-0023 and ANR-11-IDEX-0005-02), and the ANR through a chaire
635 d'excellence Sorbonne Paris Cité.
636
637 **REFERENCES**
638 Albarède, F., Albalat, E., Lee, C.T.A. (2015) An intrinsic volatility scale relevant to the
639 Earth and Moon and the status of water in the Moon. Meteoritics & Planetary Science
640 50, 568-577.
641 Bass, M.N. 1972. Description of 66095. In: Apollo 16 Lunar Sample Information
642 Catalog, 268-274. MSC-03210, NASA Johnson Space Center, Houston.
643 Bonnand, P., Parkinson, I.J., Anand, M., 2016. Mass dependent fractionation of stable
644 chromium isotopes in mare basalts: implications for the formation and the
645 differentiation of the Moon. Geochimica et Cosmochimica Acta, 175, 208-221.
646 Boyce, J.W., Treiman, A.H., Guan, Y., Ma, C., Eiler, J.M., Gross, J., Greenwood, J.P.,
647 Stolper, E.M., 2015. The chlorine isotope fingerprint of the lunar magma ocean.
648 Science advances, 1, e1500380.
649 Chen, Y., Zhang, Y., Liu, Y., Guan, Y., Eiler, J., Stolper, E.M., 2015. Water, fluorine,
650 and sulfur concentrations in the lunar mantle. Earth and Planetary Science Letters 427,
651 37-46.
652 Colson, R.O., 1992. Mineralization on the moon? Theoretical considerations of Apollo 16
653 'rusty rocks', sulfide replacement in 67016, and surface-correlated volatiles on lunar
654 volcanic glass. Lunar and Planetary Science Conference Proceedings, 22, 427-436.

655 Colaprete, A., Schultz, P., Heldmann, J., Wooden, D., Shirley, M., Ennico, K., Hermalyn,
656 B., Marshall, W., Ricco, A., Elphic, R.C., Goldstein, D., 2010. Detection of water in
657 the LCROSS ejecta plume. Science, 330, 463-468.
658 Craddock, P.R., Warren, J.M. and Dauphas, N., 2013. Abyssal peridotites reveal the near-
659 chondritic Fe isotopic composition of the Earth. Earth and Planetary Science Letters,
660 365, 63-76.
661 Day, J.M.D. 2018. Geochemical constraints on residual metal and sulfide in the sources
662 of lunar mare basalts. American Mineralogist, 103, 1734-1740.
663 Day, J.M.D., Moynier, F. 2014. Evaporative fractionation of volatile stable isotopes and
664 their bearing on the origin of the Moon. Phil. Trans. R. Soc. London Ser. A 372, 2024,
665 20130259.
666 Day, J.M.D., Walker, R.J. 2015. Highly siderophile element depletion in the Moon. Earth
667 and Planetary Science Letters, 423, 114-124.
668 Day J.M.D., Pearson D.G., Taylor L.A., 2007. Highly siderophile element constraints on
669 accretion and differentiation of the Earth-Moon system. Science, 315, 217-219.
670 Day, J.M.D., Qin, L., Ash, R.D., McDonough, W.F., Teng, F.-Z., Rudnick, R.L., Taylor,
671 L.A. 2016. Evidence for high-temperature fractionation of lithium isotopes during
672 differentiation of the Moon. Meteoritics and Planetary Science, 51, 1046-1062.
673 Day, J.M.D., Moynier, F., Shearer, C.K. 2017. Late-stage magmatic outgassing from a
674 volatile-depleted Moon. Proceedings of the National Academy of Sciences, 114, 9457-
675 9551.
676 Dhaliwal, J.K., Day, J.M.D., Moynier, F., 2018. Volatile element loss during planetary
677 magma ocean phases. Icarus, 300, 249-260.
678 Ebihara, M., Wolf, R., Warren, P.H., Anders, E., 1992. Trace elements in 59 mostly
679 highland moon rocks. In Lunar and Planetary Science Conference Proceedings 22,
680 417-426.
681 Epstein, S., Taylor Jr, H.P., 1974. D/H and O-18/O-16 ratios of H^2O in the 'rusty' breccia
682 66095 and the origin of 'lunar water'. Lunar and Planetary Science Conference
683 Proceedings, 5, 1839-1854).
684 Feldman, W.C., Maurice, S., Binder, A.B., Barraclough, B.L., Elphic, R.C., Lawrence,
685 D.J., 1998. Fluxes of fast and epithermal neutrons from Lunar Prospector: Evidence
686 for water ice at the lunar poles. Science, 281, 1496-1500.
687 Garrison, J.R., Taylor, L.A. 1980. Genesis of highland basalt breccias: a view from
688 66095. In: Papike J.J., Merrill, M., Eds. Proceedings of the Conference on the Lunar
689 Highlands Crust, Geochimica et Cosmochimica Supplement, 12, 395-417.
690 Hauri, E.H.,Weinreich, T., Saal, A., Rutherford, M., Van Orman, J.A., 2011. High Pre-
691 Eruptive Water Contents Preserved in Lunar Melt Inclusions. Science, 333, 213-215.
692 Herzog, G.F., Moynier, F., Albarède, F., Berezhnoy, A.A., 2009. Isotopic and elemental
693 abundances of copper and zinc in lunar samples, Zagami, Pele's hairs, and a terrestrial
694 basalt. Geochimica et Cosmochimica Acta 73, 5884-5904.
695 Hill, P., Schauble, E.A., 2008. Modeling the effects of bond environment on equilibrium
696 iron isotope fractionation in ferric aquo–chloro complexes. Geochimica et
697 Cosmochimica Acta, 72, 1939–1958.
698 Hunter, R.H., Taylor, L.A. 1981. Rusty rock 66095: a paradigm for volatile-element
699 mobility in highland rocks. Proceedings of the 12th Lunar and Planetary Science
700 Conference, 261-280.

701 Jean, M.M., Bodnar, R., Farley, C., Taylor, L.A. 2016. 'Rusty Rocks' from the Moon:
702 Volatile-Element Contributions from Meteorites. Lunar and Planetary Science
703 Conference, 47, 2498.
704 Jones, J.H., Palme, H., 2000. Geochemical constraints on the origin of the Earth and
705 Moon. In: Canup, R.M., Righter, K. (Eds.) Origin of the Earth and Moon, University
706 of Arizona Press, Tucson, 197-216.
707 Jovanovic S., Reed G.W. 1981. Aspects of the history of 66095 based on trace elements
708 in clasts and whole rock. Proc. 12th Lunar Planet. Sci. Conf. 295-304.
709 Kato, C., Moynier, F., Valdes, M.C., Dhaliwal, J.K., Day, J.M.D. 2015. Extensive
710 volatile loss during formation and differentiation of the Moon. Nature
711 Communications, 6.
712 Krahenbuhl, U., Ganapathy, R., Morgan, J.W., Anders, E. 1973. Volatile elements in
713 Apollo 16 samples: Implications for highland volcanism and accretion history of the
714 moon. Proc. 4th Lunar Sci. Conf. 1325-1348.
715 Li, S., Milliken, R.E., 2017. Water on the surface of the Moon as seen by the Moon
716 Mineralogy Mapper: Distribution, abundance, and origins. Science advances, 3,
717 p.e1701471.
718 Liu Y., Spicuzza M.J., Craddock P.D., Day J.M.D., Valley J.W., Dauphas N., Taylor
719 L.A. 2010. Oxygen and iron isotope constraints on near-surface fractionation effects
720 and the composition of lunar mare basalt source regions. Geochimica et
721 Cosmochimica Acta, 74, 6249-6262.
722 Lindsay, F.N., Herzog, G.F., Albarède, F., Korotev, R.L., 2011, Elemental and Isotopic
723 Abundances of Fe, Cu and Zn in Low-Ti Basalts. Lunar and Planetary Science
724 Conference, 42, 1907.
725 Lodders, K., 2003. Solar system abundances and condensation temperatures of the
726 elements. The Astrophysical Journal, 591, 1220.
727 Ma, C., Liu, Y., 2019. Discovery of zinc-rich mineral on the surface of lunar orange
728 pyroclastic beads. American Mineralogist 10.2138/am-2019-6896.
729 Maréchal, C.N., Télouk, P., Albarède, F., 1999. Precise analysis of copper and zinc
730 isotopic compositions by plasma-source mass spectrometry. Chemical Geology, 156,
731 251-273.
732 McDonough, W.F., Sun, S.S., 1995. The composition of the Earth. Chemical Geology,
733 120, pp.223-253.
734 McIntosh, E.C., Day, J.M.D., Liu, Y., 2018. Insights into Impactor Populations Striking
735 the Moon from Melt Coat and Regolith Meteorite Compositions. Lunar and Planetary
736 Science Conference, 49, 2083.
737 Millet, M.A., Dauphas, N., Greber, N.D., Burton, K.W., Dale, C.W., Debret, B.,
738 Macpherson, C.G., Nowell, G.M., Williams, H.M., 2016. Titanium stable isotope
739 investigation of magmatic processes on the Earth and Moon. Earth and Planetary
740 Science Letters, 449, 197-205.
741 Moynier, F., Albarède, F., Herzog, G.F. 2006. Isotopic composition of zinc, copper, and
742 iron in lunar samples. Geochimica et Cosmochimica Acta 70, 6103–6117.
743 Moynier, F., Agranier, A., Hezel, D.C., Bouvier, A., 2010. Sr stable isotope composition
744 of Earth, the Moon, Mars, Vesta and meteorites. Earth and Planetary Science Letters,
745 300, 359-366.

746 Moynier, F., Vance, D., Fujii, T., Savage, P., 2017. The isotope geochemistry of zinc and
747 copper. Reviews in Mineralogy and Geochemistry, 82, 543-600.
748 Nunes P.D., Tatsumoto M. 1973. Excess lead in "Rusty Rock" 66095 and implications
749 for an early lunar differentiation. Science 182, 916-920.
750 O'Neill, H.S.C., 1991. The origin of the Moon and the early history of the Earth—A
751 chemical model. Part 1: The Moon. Geochimica et Cosmochimica Acta, 55, 1135-
752 1157.
753 Paige, D.A., Siegler, M.A., Zhang, J.A., Hayne, P.O., Foote, E.J., Bennett, K.A.,
754 Vasavada, A.R., Greenhagen, B.T., Schofield, J.T., McCleese, D.J., Foote, M.C.,
755 2010. Diviner lunar radiometer observations of cold traps in the Moon's south polar
756 region. Science, 330, 479-482.
757 Paniello, R.C., Day, J.M.D., Moynier, F. 2012. Zinc isotopic evidence for the origin of
758 the Moon. Nature 490, 376-379.
759 Papanastassiou, D.A., Wasserburg, G.J., Burnett, D.S., 1970. Rb-Sr ages of lunar rocks
760 from the Sea of Tranquillity. Earth and Planetary Science Letters, 8, 1-19.
761 Pieters, C.M., Goswami, J.N., Clark, R.N., Annadurai, M., Boardman, J., Buratti, B.,
762 Combe, J.P., Dyar, M.D., Green, R., Head, J.W., Hibbitts, C., 2009. Character and
763 spatial distribution of OH/H_2O on the surface of the Moon seen by M3 on
764 Chandrayaan-1. Science, 326, 568-572.
765 Poitrasson, F., Halliday, A.N., Lee, D.C., Levasseur, S., Teutsch, N., 2004. Iron isotope
766 differences between Earth, Moon, Mars and Vesta as possible records of contrasted
767 accretion mechanisms. Earth and Planetary Science Letters, 223, 253-266.
768 Poitrasson, F., Delpech, G., Grégoire, M., 2013. On the iron isotope heterogeneity of
769 lithospheric mantle xenoliths: implications for mantle metasomatism, the origin of
770 basalts and the iron isotope composition of the Earth. Contributions to Mineralogy and
771 Petrology, 165, 1243-1258.
772 Polyakov, V.B., Soultanov, D.M., 2011. New data on equilibrium iron isotope
773 fractionation among sulfides: Constraints on mechanisms of sulfide formation in
774 hydrothermal and igneous systems. Geochimica et Cosmochimica Acta, 75, 1957-
775 1974.
776 Pringle, E.A., Moynier, F., 2017. Rubidium isotopic composition of the Earth, meteorites,
777 and the Moon: Evidence for the origin of volatile loss during planetary accretion.
778 Earth and Planetary Science Letters, 473, 62-70.
779 Renggli, C.J., King, P.L., Henley, R.W., Norman, M.D., 2017. Volcanic gas composition,
780 metal dispersion and deposition during explosive volcanic eruptions on the Moon.
781 Geochimica et Cosmochimica Acta, 206, 296-311.
782 Ringwood, A.E., Kesson, S.E., 1977. Basaltic magmatism and the bulk composition of
783 the Moon. The Moon, 16, 425-464.
784 Schultz, P.H., Staid, M.I., Pieters, C.M., 2006. Lunar activity from recent gas release.
785 Nature, 444, 184-187.
786 Scott, S. D., 1983. Chemical behaviour of sphalerite and arsenopyrite in hydrothermal
787 and metamorphic environments. Mineralogical Magazine 47, 427-435.
788 Sedaghatpour, F., Teng, F.Z., Liu, Y., Sears, D.W., Taylor, L.A., 2013. Magnesium
789 isotopic composition of the Moon. Geochimica et Cosmochimica Acta, 120, 1-16.

Sharp, Z.D., Shearer, C.K., McKeegan, K.D., Barnes, J.D., Wang, Y.Q. 2010. The chlorine isotope composition of the Moon and implications for an anhydrous mantle. Science 329, 1050-1053.

Shearer, C.K., Sharp, Z.D., Burger, P.V., McCubbin, F.M., Provencio, P.P., Brearley, A.J., Steele, A. 2014. Chlorine distribution and its isotopic composition in "rusty rock" 66095. Implications for volatile element enrichments of "rusty rock" and lunar soils, origin of "rusty" alteration, and volatile element behavior on the Moon. Geochimica et Cosmochimica Acta 139, 411-433.

Sisson, T.W., Grove, T.L., 1993. Experimental investigations of the role of H_2O in calc-alkaline differentiation and subduction zone magmatism. Contributions to Mineralogy and Petrology, 113, 143-166.

Sossi, P.A., Moynier, F., 2017. Chemical and isotopic kinship of iron in the Earth and Moon deduced from the lunar Mg-suite. Earth and Planetary Science Letters, 471, 125-135.

Sossi, P.A., Halverson, G.P., Nebel, O., Eggins, S.M., 2015. Combined separation of Cu, Fe and Zn from rock matrices and improved analytical protocols for stable isotope determination. Geostandards and Geoanalytical Research, 39, 129-149.

Sossi, P.A., Nebel, O. and Foden, J., 2016. Iron isotope systematics in planetary reservoirs. Earth and Planetary Science Letters, 452, 295-308.

Sossi, P.A., Moynier, F., Van Zuilen, K., 2018. Volatile loss following cooling and accretion of the Moon revealed by chromium isotopes. Proceedings of the National Academy of Sciences, 115, 10920-10925.

Spicuzza M.J., Day J.M.D., Taylor L.A., Valley J.W., 2007. Oxygen isotope constraints on the origin and differentiation of the Moon. Earth and Planetary Science Letters, 253, 254-265.

Syverson, D.D., Luhmann, A.J., Tan, C., Borrok, D.M., Ding, K., Seyfried Jr, W.E., 2017. Fe isotope fractionation between chalcopyrite and dissolved Fe during hydrothermal recrystallization: An experimental study at 350° C and 500 bars. Geochimica et Cosmochimica Acta, 200, 87-109.

Tatsumoto, M., Rosholt, J.N., 1970. Age of the moon: An isotopic study of uranium-thorium-lead systematics of lunar samples. Science, 167, 461-463.

Tatsumoto, M., Premo, W., Unruh, D.M., 1987. Origin of lead from green glass of Apollo 15426: A search for primitive lunar lead. Proc. 17th Lunar Planet. Sci. Conf., JGR 92, E361-E371.

Taylor, L.A., 2012. Water, Water, Everywhere: But How to Find and Use It on the Moon! Annual Meeting of the Lunar Exploration Analysis Group 1685

Taylor L.A., Mao H.K., Bell P.M., 1973. "Rust" in the Apollo 16 rocks. Proc. 4th Lunar Sci. Conf. 829-839.

Taylor, L.A., Mao, H.K., Bell, P.M., 1974. Beta-FeOOH, akaganeite, in lunar rocks. In Lunar and Planetary Science Conference Proceedings, 5, 743-748.

Valdes, M.C., Moreira, M., Foriel, J., Moynier, F., 2014. The nature of Earth's building blocks as revealed by calcium isotopes. Earth and Planetary Science Letters, 394, 135-145.

Walker, R.J., Horan, M.F., Shearer, C.K., Papike, J.J., 2004. Low abundances of highly siderophile elements in the lunar mantle: evidence for prolonged late accretion. Earth and Planetary Science Letters, 224, 399-413.

836 Wang, K., Jacobsen, S.B., 2016. Potassium isotopic evidence for a high-energy giant
837 impact origin of the Moon. Nature, 538, 487-490.
838 Wang, K., Moynier, F., Podosek, F.A., Foriel, J., 2012. An iron isotope perspective on
839 the origin of the nanophase metallic iron in lunar regolith. Earth and Planetary Science
840 Letters, 337, 17-24.
841 Wang, K., Jacobsen, S.B., Sedaghatpour, F., Chen, H., Korotev, R.L., 2015. The earliest
842 Lunar Magma Ocean differentiation recorded in Fe isotopes. Earth and Planetary
843 Science Letters, 430, 202-208.
844 Wanke, H., Blum, K., Dreibus, G., Palme, H., Spettel, B., 1981, March. Multielement
845 Analysis of Samples from Highland Breccia 66095: A contribution to the "Rusty
846 Rock" Consortium. Lunar and Planetary Science Conference, 12, 1136-1138.
847 Weyer, S., Anbar, A.D., Brey, G.P., Münker, C., Mezger, K., Woodland, A.B., 2005. Iron
848 isotope fractionation during planetary differentiation. Earth and Planetary Science
849 Letters, 240, 251-264.
850 Wolf, R., Anders, E., 1980. Moon and Earth: compositional differences inferred from
851 siderophiles, volatiles, and alkalis in basalts. Geochimica et Cosmochimica Acta, 44,
852 2111-2124.
853 Young, E.D., Kohl, I.E., Warren, P.H., Rubie, D.C., Jacobson, S.A. and Morbidelli, A.,
854 2016. Oxygen isotopic evidence for vigorous mixing during the Moon-forming giant
855 impact. Science, 351, 493-496.

Figures and Figure Captions

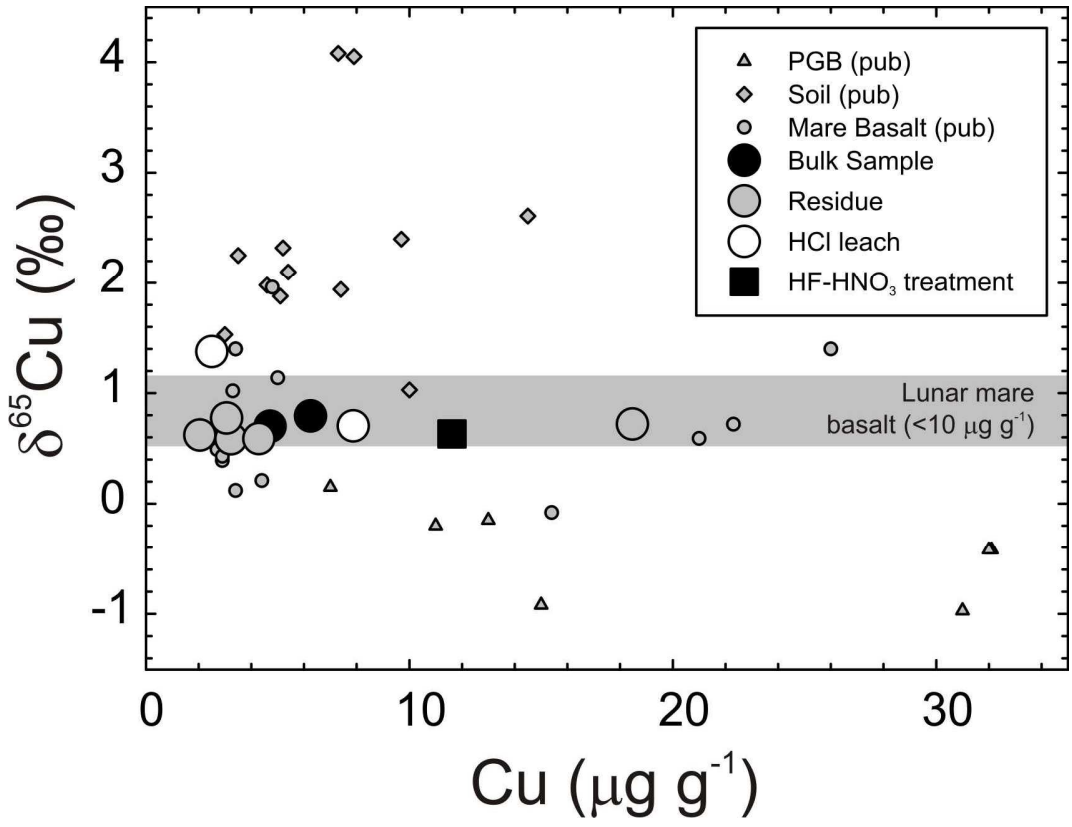

Figure 1: Copper content versus Cu isotopic composition for compositions measured in 66095. Shown is the lunar mare basalt average estimate filtering samples with less than 10 µg g^{-1} Cu, from a compilation of published (pub) data from Moynier et al. (2006), Herzog et al. (2009), and Lindsay et al. (2011). PGB are lunar pyroclastic glass beads.

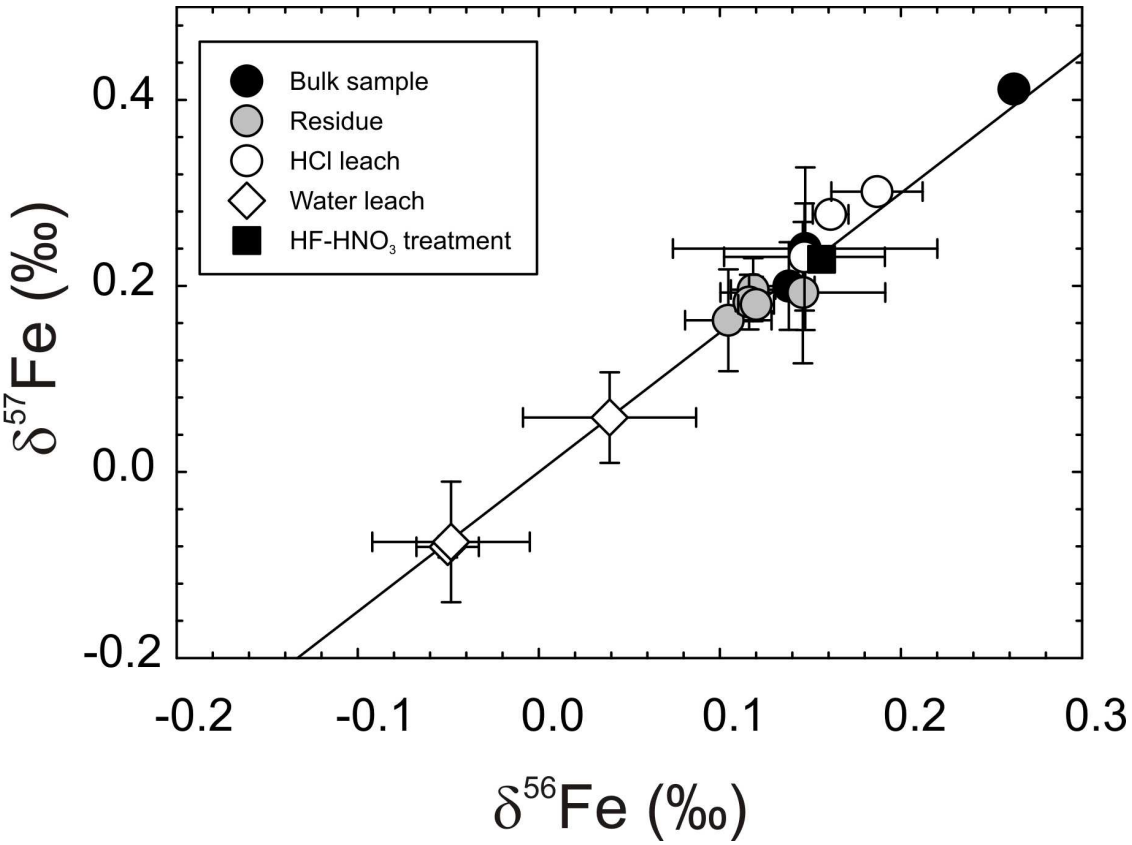

Figure 2: Three-isotope iron plot for compositions measured in 66095. All samples fall on the mass-dependent slope of 1.5.

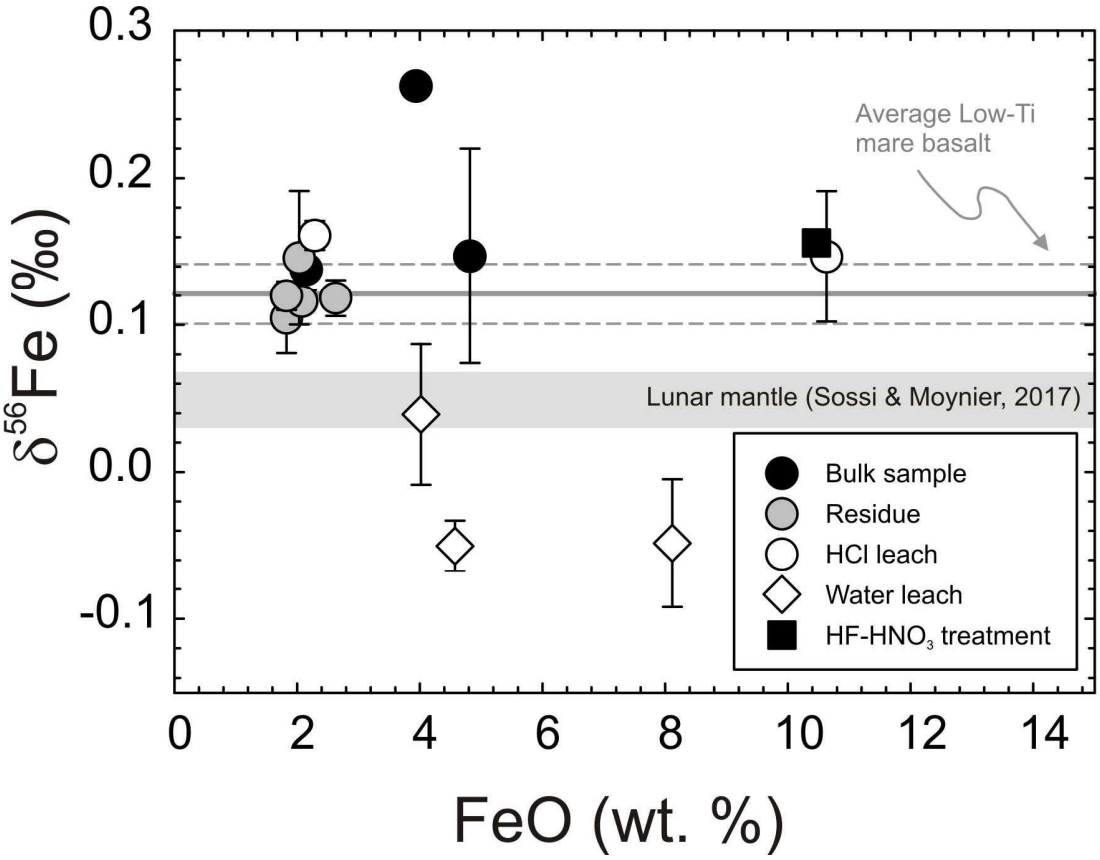

Figure 3: Iron content versus Fe isotopic composition for compositions measured in 66095. Shown for comparison is the lunar mantle estimate of Sossi & Moynier (2017), and the average low-Ti mare basalt composition from a compilation of data from Poitrasson et al. (2004), Weyer et al. (2005), Liu et al. (2010), Wang et al. (2015) and Sossi & Moynier (2017).

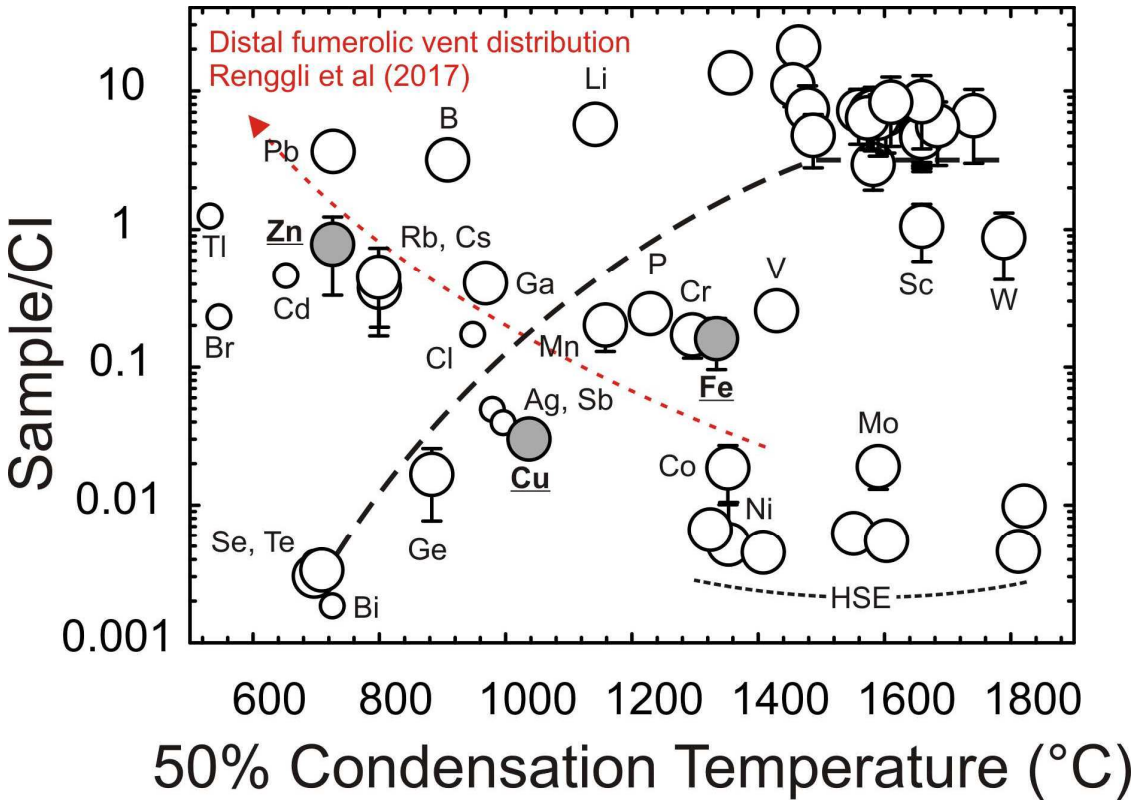

875
876
877 **Figure 4:** Plot of 50% Condensation Temperature versus the average compositions of
878 breccia and anorthosite components in 66095, 421, 66095, 425 and 66095, 430 (from
879 Day et al., 2017; large symbols) along with published Tl, Br, Cd, Bi, Cl, Ag and Sb data
880 for 66095 from Krahenbuhl et al. (1973) and Sharp et al. (2010) (smaller symbols),
881 normalized to CI chondrite. Highlighted in grey are the Cu, Fe and Zn abundances. The
882 dashed line is the average lunar volatile depletion trend using data from O'Neill (1991),
883 and red dashed line is the predicted deposition of metals within a lunar
884 fumarolic/volcanic gas distal from the source from Renggli et al. (2017). Condensation
885 temperature values are from Lodders (2003) and CI chondrite normalization is from
886 McDonough & Sun (1995).

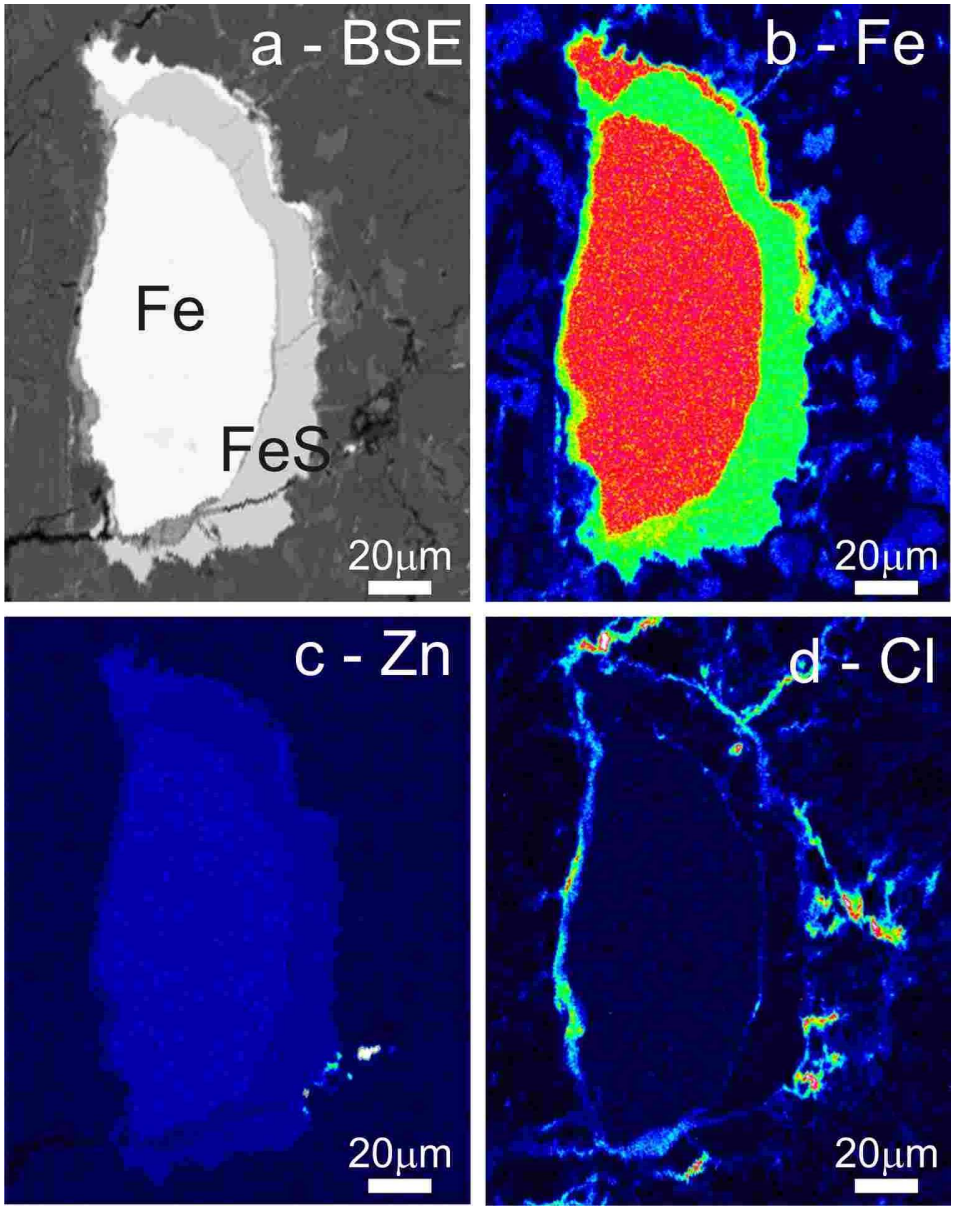

Figure 5: Location of elements within metal and sulfide grains in the 'Rusty Rock', 66095. Warmer and brighter colours correspond to higher concentrations. Iron occurs dominantly within FeNi metal in the sample, whereas Zn is hosted dominantly in sphalerite, and Cl occurs within veins and fractures. (a) Back-Scatter Electron (BSE) image showing primary mineralogy and crystalline texture. Wave-length Dispersive Spectrum (WDS) images of (b) Fe, (c) Zn distribution within sphalerite (bright phase) and (d) Cl distribution within fractures and around metal grains. Fe = metal, FeS = troilite. Image adapted from Day et al. (2017).

Table 1: Iron, copper and zinc isotope data for the 'Rusty Rock' 66095

Sample	Lithology	Type	Experiment	Lab ID	Mass (g)	FeO (wt.%)[a]	FeO (wt.%)	δ^{56}Fe	±2SE	δ^{57}Fe	±2SE	n	Cu µg g^{-1} [a]	Cu µg g^{-1}	δ^{65}Cu	±2SE	n	Zn µg g^{-1}	δ^{66}Zn	±2σ	δ^{67}Zn	±2σ	δ^{68}Zn	±2σ
66095, 421	Breccia	Bulk	Bulk	J1	0.01570	4.5	4.8	0.15	0.07	0.24	0.09	2	3.56	4.71	0.70	0.06	2	102	-13.53	0.05	-20.19	0.11	-26.88	0.10
		Residue (J14)	Exp. 2	J12	0.01340		1.8	0.10	0.02	0.16	0.05	2		18.5	0.72	0.01	2	100	-13.58	0.05	-20.25	0.08	-26.96	0.08
		1M HCl Leach	Exp. 2	J14	0.00900		2.3	0.16	0.01	0.28	0.01	2		2.50	1.38	0.01	2	52.4	-13.27	0.06	-19.81	0.08	-26.34	0.08
		Residue (RR)	Exp. 3	RR1	0.02741		2.6	0.12	0.01	0.20	0.03	2		2.04	0.62	0.03	2	14.8	-13.72	0.03	-20.41	0.06	-27.20	0.06
		20min H_2O US	Exp. 3	RR2	0.00064		4.0	0.04	0.05	0.06	0.05	2						395	-8.14	0.31	-12.15	0.42	-16.14	0.65
		20min 3N HCl US	Exp. 3	RR3	0.00610		10.6	0.15	0.04	0.23	0.06	2		7.87	0.70	0.02	2	210	-13.26	0.05	-19.79	0.07	-26.33	0.09
		2hr 1N HF-HNO_3	Exp. 3	RR4	0.00482		10.5	0.16	0.01	0.23	0.00	2		11.6	0.63	0.05	2	165	-13.40	0.01	-19.98	0.05	-26.60	0.01
66095, 425 (A)	Anorthosite	Bulk	Bulk	J2	0.00670	2.0	2.2	0.14	0.01	0.20	0.05	2	3.64					397	-13.52	0.07	-20.17	0.10	-26.84	0.13
66095, 425 (B)	Anorthosite	Residue (LP1)	Exp. 1	J3	0.00620	2.4	2.0	0.15	0.05	0.19	0.08	2	3.61	3.23	0.59	0.05	2	325	-13.53	0.03	-20.20	0.06	-26.87	0.06
		30min H_2O	Exp. 1	LP1	0.00002		4.6	-0.05	0.02	-0.08	0.01	2						12043	-13.32	0.05	-19.88	0.10	-26.46	0.09
66095, 430	Breccia	Bulk	Bulk	J4	0.00640	5.5	3.9	0.26	0.01	0.41	0.00	2	5.42	6.25	0.79	0.03	2	397	-13.98	0.06	-20.86	0.11	-27.76	0.11
		Residue (LP2)	Exp. 1	J5	0.00980	4.5	2.1	0.12	0.01	0.18	0.03	2	2.90	3.06	0.77	0.07	2	260	-13.02	0.05	-19.40	0.12	-25.83	0.08
		30min H_2O	Exp. 1	LP2	0.00003		8.1	-0.05	0.04	-0.08	0.06	2						2577	-12.34	0.04	-18.28	0.07	-24.33	0.04
		Residue (J15)	Exp. 2	J13	0.00770		1.8	0.12	0.01	0.18	0.01	2		4.29	0.59	0.04	2	278	-13.80	0.03	-20.60	0.05	-27.40	0.05
		1M HCl Leach	Exp. 2	J15	0.00013	2.7	24.6	0.19	0.03	0.30	0.00	2	2.71					6709	-13.28	0.05	-19.82	0.07	-26.39	0.08
Milhas Hematite Standard (ETH)								0.51	0.02	0.75	0.02	6												
BHVO-2 (USGS)															0.07	0.06	2							

[a]FeO, Cu and all Zn abundances and isotopic data were previously reported in Day et al. (2017). US = ultra-sonification

Table 2: Mass balance calculations for Fe, Cu and Zn systematics in 66095

Sample	Experiment	Detail	Lab ID	Mass (g)	Fraction	∑FeO (wt.%)	$\sum\delta^{56}Fe$	∑Cu (μg g^{-1})	$\sum\delta^{65}Cu$	∑Zn (μg g^{-1})	$\sum\delta^{66}Zn$
66095, 421	Bulk		J1	0.01570	100%	4.82	0.15	4.71	0.70	102.1	-13.5
	Exp. 2	Residue (J14)	J12	0.01340	59.8%	2.01	0.13	12.05	0.98	81.1	-13.5
	Exp. 2	1M HCl Leach	J14	0.00900	40.2%						
	Exp. 3	Residue (RR)	RR1	0.02741	70.3%	4.87	0.13	4.11	0.63	70.1	-13.5
	Exp. 3	20min H_2O US	RR2	0.00064	1.6%						
	Exp. 3	20min 3N HCl US	RR3	0.00610	15.7%						
	Exp. 3	2hr 1N HF-HNO_3	RR4	0.00482	12.4%						
66095, 425 (A)	Bulk		J2	0.00670	100%	2.15	0.14			397.4	-13.5
66095, 425 (B)	Exp. 1	Residue (LP1)	J3	0.00620	99.6%	2.04	0.15	3.23	0.59	366.5	-13.5
	Exp. 1	30min H_2O	LP1	0.00002	0.4%						
66095, 430	Bulk		J4	0.00640	100%	3.94	0.26	6.25	0.79	396.7	-14.0
	Exp. 1	Residue (LP2)	J5	0.00980	99.7%	2.10	0.12	3.06	0.77	267.7	-13.0
	Exp. 1	30min H_2O	LP2	0.00003	0.3%						
	Exp. 2	Residue (J15)	J13	0.00770	98.3%	2.21	0.12	4.21	0.59	384.6	-13.8
	Exp. 2	1M HCl Leach	J15	0.00013	1.7%						

US = ultra-sonification